ORIGINAL RESEARCH ARTICLE

A Homogenization Technology for Heavy Ingots: Hot-Top Pulsed Magneto-Oscillation

HONGGANG ZHONG, LIXIN ZHOU, HUAZHI YUAN, KE HAN, QINGYOU HAN, ZHISHUAI XU, LIJUAN LI, FAN ZHANG, JIAN HUANG, RENXING LI, and QIJIE ZHAI

We scaled up a previously developed method, known as Hot-top Pulsed Magneto-Oscillation (HPMO), to minimize crack, shrinkage-cavity, and macrosegregation in large ingots. Simulations on electromagnetic field, flow field, and temperature field revealed that an HPMO-induced electromagnetic field forces circulation of liquid steel near the riser, which causes grain nuclei and free grains to fall off the riser walls, drift away, and settle onto the middle of the mold. This phenomenon, known as ''grain showering'', refines solidified structure and reduces segregation. Joule heating generated by the HPMO process leads to mass feeding of the riser, which eliminates the development of pipes or central porosity and cracks. Based on simulation results, we designed a prototype HPMO apparatus and tested it on the production of ingots weighing 18 tonnes. Experimental results indicated that the use of HPMO grain showering did indeed yield expected solidified structure in ingots with a 56–83 pct reduction in equiaxed grain size, a 41 pct reduction in the number of inclusions, and a 50–75 pct reduction in normal carbon segregation comparing with that in controlled ingots. Furthermore, by using HPMO, shrinkage-induced pipes and center cracks that often occurred in the control ingots were eliminated, resulting in a fourfold increase in ductility in critical regions of the ingot. This work demonstrated the value of computation-aided simulation for improving manufacturing methods for the casting of large ingots.

HONGGANG ZHONG, HUAZHI YUAN, ZHISHUAI XU, LIJUAN LI, FAN ZHANG, RENXING LI, and QIJIE ZHAI are with the Center for Advanced Solidification Technology, Shanghai University, Shanghai 200072, P.R. China; LIXIN ZHOU and JIAN HUANG are with the Daye Special Steel Co. LTD, Huangshi, Hubei 214429, P.R. China; KE HAN is with the National High Magnetic Field Laboratory, 1800 E. Paul Dirac Drive, Tallahassee, FL, 32310–3706; QINGYOU HAN is with the School of Mechanical Engineering, Southeast University, Nanjing 211189, P.R. China. Contact e-mail: hgzhong@shu.edu.cn; qjzhai@shu.edu.cn

Manuscript submitted November 3, 2023; accepted January 10, 2024.

Article published online February 29, 2024.

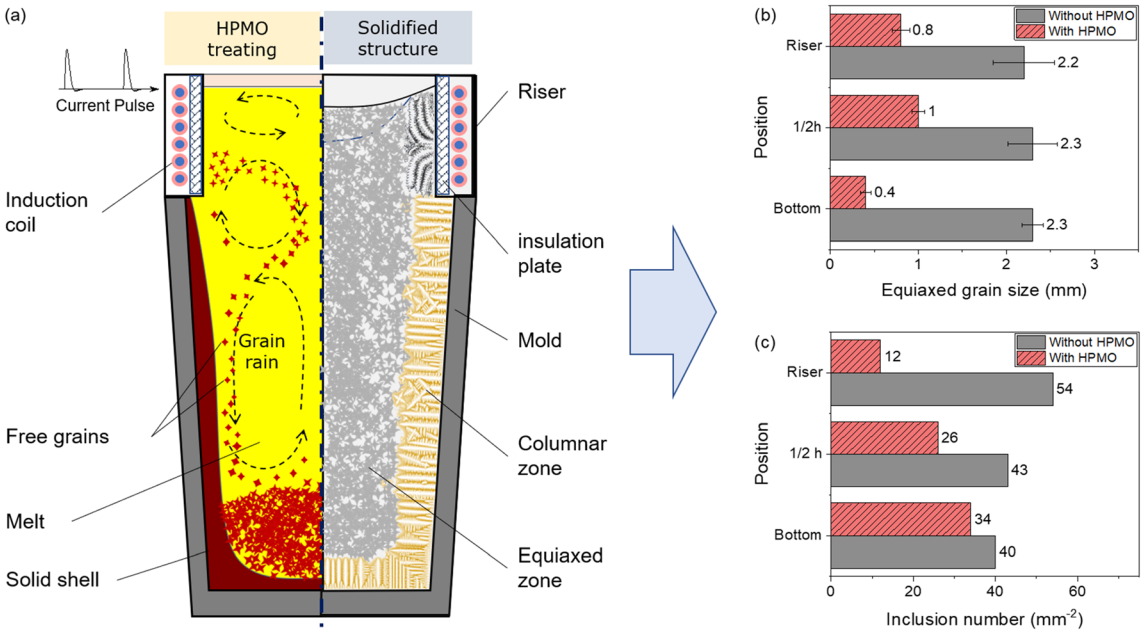

https://doi.org/10.1007/s11663-024-03019-z

I. INTRODUCTION

LARGE parts manufactured by forging have long been employed in the nuclear power and hydropower industries, as well as in the manufacture of mining machinery. For these applications, the casting process of heavy ingots (those composed of the parent metal of forgings) must be strictly controlled to ensure quality. Macroscopic defects that commonly occur in heavy ingots, such as coarse dendritic grains, severe macrosegregation, porosity, and cracks, have to be mitigated which not only decreases product yield but also increases the cost of production by increasing the duration of required heat treatment and the number of required fabrication steps. The existence of macroscopic defects in ingots is also a safety hazard and wastage. Lesoult[1] revealed that typical macroscopic defects in a 65-tonnes steel ingot were negative segregates of equiaxed grains in a cone-shaped settling zone at the bottom of the ingot, normal segregation and shrinkage-induced porosity in the top layer of the ingot (near the riser section of the mold), and channel segregation in the middle. These results were generally consistent with other reports. Flemings[2,3] concluded that the primary causes of macrosegregation were the flow of solute-rich liquid between dendritic grains combined with the movement of free grains throughout the melt. Li *et al.*[4] found that channel segregation is aggravated by buoyancy induced flow whenever the volume fraction of oxide inclusions reaches a certain value. Eskin *et al.*[5] proposed that grain refinement is beneficial for improving the central negative segregation of the billet.

Reducing grain size is known to be beneficial in enhancing the strength and ductility of cast ingots by increasing the mass feeding effect to reduce porosity formation, by reducing macrosegregation, and by reducing stresses and increasing strength of the mushy alloy to prevent crack formation. As a result, ingots of small grains are more homogeneous in their solidification microstructure, easier to be hot worked, and higher in quality in the resultant forgings than that of corse grains. Consequently, metallurgists have developed a variety of methods to control ingot solidification, including using—exothermic risers,[6–8] multi-pouring processes,[9] mechanical oscillations,[10,11] adding chilling balls,[12] ultrasonic treatments,[13–16] electromagnetic stirring,[17–19] and pulsed currents.[20–22] Exothermic risers have been found to decrease shrinkage by enhancing feeding effects, and multi-pouring processes have been found to reduce macrosegregation by controlling the composition of molten steel of each ladle. Recently, Li *et al.*[23,24] proposed a layer-by-layer casting method that would enable ingot fabrication while clearly restraining multiphase flow and reducing solute segregation. Other technologies have been developed to increase the number of equiaxed grain nuclei. However, most of these technologies have proved to be impractical in grain refining of large steel ingots which are associated with high temperatures, low cooling rates, heavy tonnage, and thick casting molds. To our knowledge,

the problems of macrosegregation, porosity, and cracks in industrial heavy ingots (*i.e.*, tens to hundreds of tonnes) have not yet been fully resolved.

Pulsed magneto-oscillation (PMO)[25] promotes nucleation at the freezing front through inductive effects caused by the pulsed current in the coils wound around the outside of an ingot. This can effectively refine the solidified ingot structure and decrease macrosegregation. Considering the significant application prospects of PMO in the field of ingot solidification, Zhao *et al.* have studied several PMO treatment methods that are suitable for ingots, including surface-type and riser-type approaches. They found[26] that the a pure Al ingot treated via PMO with coils placed near the risers attained a completely equiaxed grain structure, with a mean grain size of approximately 240 μm. On this basis, Li *et al.*[27] treated a 150-kg steel ingot using a technique known as Hot-top Pulsed Magneto-Oscillation (HPMO). They found that the homogenization and compactness of the solidified structure were improved significantly. However, for steel ingots weighing tens to hundreds of tonnes, the HPMO process should be optimized through further simulations and industrial experiments. For example, it is unknown whether free grains formed near the riser could be deposited as sediment at the bottom of the heavy ingot (layer-by-layer until reaching the top), or whether the normal segregation in riser would increase due to the grain showering and buoyancy, or when is the best time to apply PMO.

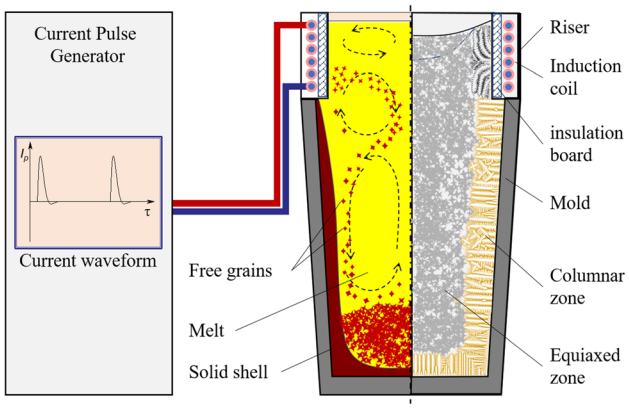

Fig. 1—Schematic illustrations of experimental setup, circulation patterns and microstructure formation within a solidifying ingot subject to HPMO.

In this study, the possibility of improving heavy ingot homogenization by employing HPMO was investigated using numerical simulations and industrial experimental tests. The results confirm that the central microstructure and macrosegregation in an 18-tonne steel ingot were improved by using HPMO.

II. STRATEGY FOR IMPROVING HEAVY INGOT HOMOGENIZATION *VIA* HPMO

Because pulsed electrical current refines grains by increasing nucleation rates, the optimal time to introduce this current is during the nucleation stage when metal solidification happens.[28] Application of PMO for a non-contact treatment to refine grains has been done by transmitting pulsed electrical current through an induction coil.[25] Similar to the pulsed electrical current method, the grain refining mechanism of PMO is also associated with increasing nucleation rates and promoting the formation of free grains. PMO is suitable for industrial applications because it is a non-contact and non-contamination process that requires low energy consumption and simple operations. To make the process compatible with existing industrial production processes, we implemented PMO at the riser on the top of the molds(thus making it an HPMO strategy) to obtain heavy ingots comprising fine, uniform grains, without porosity or cracks (Figure 1).

In our designed system for heavy ingot casting shown in Figure 1, induction coils surrounding the riser generate electrical current pulses in the melt. Electromagnetic induction heating and pulsed magneto-oscillation occur in the liquid steel near the riser, enhancing heat preservation in the vicinity of the riser and promoting the nucleation of grains.[25] Inductive Lorentz forces cause the melt to adopt upper and lower circulation patterns. PMO-induced nuclei near the riser and existing free grains are driven toward the center of the melt by the lower circulation pattern, and then settled as a result of gravity and convection. Consequently, nucleated sediments are deposited layer-by-layer, forming a fine equiaxed grain zone in the entire ingot body, which significantly reduces macrosegregation and stress. Nevertheless, this HPMO treatment may result in solute enrichment near the upper part of the riser because of selective solidification and grain showering. Such solute enrichment is not an issue since the riser would be cut off from the ingot before the ingot is processed further.

Table I. The Composition of 18CrNiMo (wt pct)

C	Si	Mn	Cr	Ni	Mo	S	P	Fe
0.18	0.3	0.7	1.65	1.55	0.3	≤0.035	≤0.035	Balance

Table II. Thermophysical Properties of 18CrNiMo Gear Steel

Thermophysical Properties	Values
Viscosity (Pa·s)	5.6×10^{-3}
Conductivity ($S\cdot m^{-1}$)	1.64×10^{6}
Relative Permeability	1
Relative Conductance	1
Density ($kg\cdot m^{-3}$)	7200

III. NUMERICAL SIMULATIONS OF INDUSTRIAL TESTS

In this study, numerical simulations and industrial tests were performed for a heavy ingot treated by HPMO to verify the refining assumption discussed in Sect. II. The industrial tests were carried out on an 18-tonnes bottom-pouring steel ingot. The material was 18CrNiMo gear steel. Its composition is shown in Table I.

First, a simplified two-dimensional symmetrical model was constructed to simulate the magnetic, convection and temperature fields within the 18-tonnes ingot (using commercial software COMSOL Multiphysics, 2019, COMSOL Inc., Sweden). Tables II, III, and Figure 2 present the thermophysical properties of 18CrNiMo steel, magnetic properties used in the simulation, and temperature-dependent simulated properties of the modeled steel, respectively. An equivalent-specific heat method was used to calculate the release of latent heat during solidification; specifically, the latent heat of the phase change was dispersed non-uniformly over liquid/solid zone, as shown in Figure2. Figure 3 shows the simplified equal-proportion two-dimensional symmetrical model based on the industrial ingot. The numerical model included four components: liquid steel, a riser with HPMO coils, casting molds, and air. The casting mold was divided into three sections for the purpose of accurately setting the heat transfer boundary conditions, as shown in Figure 3(a). Grids of various types and sizes were applied in different zones to save computing resources and increase the computing speed. A combination of orthogonal and non-orthogonal grids effectively avoided a sawtooth effect at the geometric boundary of the liquid steel because of the irregular geometry of the ingot. Orthogonal grids were used near the center line of the liquid steel, whereas non-orthogonal grids were used at the geometric boundary of the liquid steel. Additionally, orthogonal grids were selected for coils, owing to their regular geometry, and triangular grids were used for the other zones. The numerical simulation grid has a size of 10 mm, comprising a total of 34,207 cells, and the simulation duration was 47 h/case. The simulation was conducted on a computer equipped with an Intel(R) Xeon(R) CPU E5-2698 v3 @ 2.3 GHz (X2) processor, and 128GB of memory.

During the casting process, turbulent models are employed to consider the forced convection induced by the electromagnetic field and the natural convection within the molten metal. The k-ε model within the COMSOL turbulent module is utilized for this calculation. The magnetic field follows the Maxwell's equations, and the electromagnetic field model within the AC/DC module is selected for the computation. The magnetic field and fluid flow are directionally coupled. The fluid flow and solidification are bidirectionally coupled through the non-isothermal flow interface within the COMSOL multiphysics coupling module. In the numerical simulation, the first step involves solving for the electromagnetic field distribution status within one pulse cycle. The electromagnetic forces obtained from this solution are then used as source terms, along with Joule heating, to compute the temperature and flow fields during the solidification process.

A. *Basic Assumptions and Boundary Conditions*

To evaluate the effects of HPMO on both the temperature and the flow field in steel ingot, we constructed a continuum model based on a finite element method.[29,30] The assumptions and governing equations of the model were detailed in the electronic supplementary data file.

To optimize the computation time, the numerical simulation was divided into two steps. First, the electromagnetic distribution during one pulse period was calculated using an electromagnetic model based on Maxwell's equations.[31] The mean Lorentz force and mean Joule heat during one pulse period were also calculated.

In the electromagnetic model, it was assumed that a magnetic field could not pass through the boundary of the air domain. When the flow field was calculated, the liquid between the top of the fluid steel and the covering agent was regarded as a sliding boundary, and the wall of the mold was considered as a rigid wall. Then, at the top of the liquid steel, only the tangential flow velocity was considered, and the flow velocity perpendicular to the liquid surface was assumed to be zero. At the wall of the mold, both the tangential and normal flow velocities were zero.

The initial conditions for the model included the followings: superheat = 50 °C; pouring process was ignored; temperature of the liquid steel was uniform; initial temperature of the mold = 25 °C; peak current of HPMO = 700 K_I A; pulse frequency = 100 K_f Hz; pulse width = 2 K_P ms (where K_I, K_f, and K_P are coefficients of power system). The heat transfer boundary conditions are shown in Table IV and Figure 4.

B. *Results of Numerical Simulations*

1. *Magnetic field in the ingot during HPMO treatment*

The density of the HPMO-induced magnetic field, which was concentrated mainly at the edges of the riser, was estimated at different times for each of sixteen locations (Figure 5). The direction of the magnetic field at all locations in the melt was first upward and then downward, accompanied by phase differences. We found that, during each pulse period, strength decreased gradually as time increased. Because of the skin effect, magnetic density was clearly higher at the edges than that at the center of the melt. The density of the

Table III. Magnetic Properties Used in the Simulation

Physical Properties	18CrNiMo	Mold	Covering Agent	Riser	Coil	Air
Relative Permeability	1	400	1	1	1	1
Relative Dielectric Constant	1	5	1	1	1	1
Conductivity/S·m^{-1}	1.64×10^{6}	5×10^{6}	10	10	6×10^{7}	0

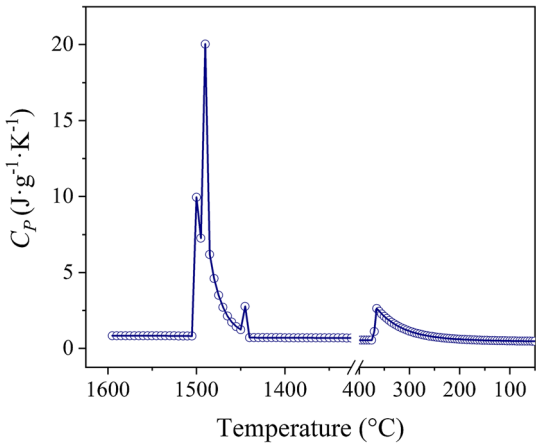

Fig. 2—Specific heat capacity as a function of temperature (computed using JMatPro).

magnetic field reached a maximum of 148 mT at 1/4 of the pulse width at the location sixteen, located near the edge of the melt.

2. *Distribution of both the Joule heat and the electromagnetic force induced by HPMO*

Because Joule heat enhances heat preservation and feeding effects, and electromagnetic force facilitates the flow of the melt, they are both important in terms of grain refinement and chemistry homogeneity of the ingot. The electromagnetic force induced by HPMO, like the magnetic field, was concentrated at the edges of the riser. The electromagnetic strength likewise decreased gradually with increasing the distance from the center of the melt to the edge, during each pulse period, reaching a maximum of 3.25×10^{5} N/m^{3} at 1/4 of the pulse period, and the electromagnetic force in the center of melt was much weaker than at the edge (Figure 6). The electromagnetic force underwent three cycles, first increasing then decreasing (accompanied by the corresponding phase differences) from the center of the melt to the edge.

We estimated the distribution of the mean Joule heat and mean electromagnetic force in the ingot during one pulse (Figure 7). We found again that the distribution of Joule heat was similar to that of electromagnetic force in that it was weaker in the center than at the edge.

3. *Flow and temperature fields comparisons*

The flow and temperature fields of 18CrNiMo gear steel were calculated with and without HPMO (Figures 8 and 9). The numerical simulation shown in Figure 9 reveals that, after cooling for 1 h, the temperatures of the steel in the ingot body without HPMO are completely lower than the liquidus. Therefore, in the industrial test, HPMO treatment was applied on the riser 1 h after pouring (*i.e.*, t = 1 h where t = 0 was the moment when, pouring was completed) to ensure that free grains can survive in the melt. The Lorentz force perpendicular to the riser wall is stronger near the wall of the riser, causes the liquid steel to flow from wall of the riser toward the center, and then either further downward or upward. As a result, upper and lower circulations are formed in the riser as shown in Figure 8. It takes 50 s for the flow field to stabilize after HPMO. However, towards the bottom of the ingot, the flow field is dominant by natural convection and is less affected by HPMO. The flow velocity is increased by about 20 pct, and the circulations induced by HPMO helps the melt wash the walls of the mold, thus increasing the grain showering effect and dendritic grain fragmentation. The grain nuclei and fragments of dendritic grains then fell to the bottom of the ingot, which is important for grain refinement. The flow velocity decreases gradually towards the bottom of the ingot because of the increasing resistance from solid dendrites and the increasing viscosity of the mushy zone. Meanwhile, the circulation zone of natural convection at the bottom of the ingot shrinks with increasing solidification times. However, the forced circulation induced by HPMO near the riser could be maintained for at least 3 h, which is beneficial for grain refinement and inclusion flotation.

Simulation results on temperature fields and fractions of solid (f_S) in ingots with and without HPMO at various times are shown in Figure 9. At the early stage of solidification (t ≤ 2 h), high-temperature melt is pushed to the edge of the riser, and low-temperature melt moves toward the center because of the forced flow induced by HPMO. As a result, the superheat of the liquid steel in HPMO ingot is decreased much quicker, and the entire melt reaches supercooled condition in 90 s after HPMO processing, which is 50 min earlier than that in the untreated ingot (at 3930 s of HPMO treated ingot & 6960 s of untreated ingot, respectively). In addition, the application of PMO can promote nucleation,[29] and drive freshly nucleated grains from regions near the riser wall towards the main body of the melt within the ingot. At the same time, free grains also exist in the supercooled melt of the ingot body. Their size must be obviously greater than the newly formed grains in the riser. Some of these free grains are brought into the molten steel in the riser about 20 s after the application of HPMO due to HPMO-induced circulations shown in Figure 8, experiencing remelting, dissolution and fragementation-induced grain multiplication.

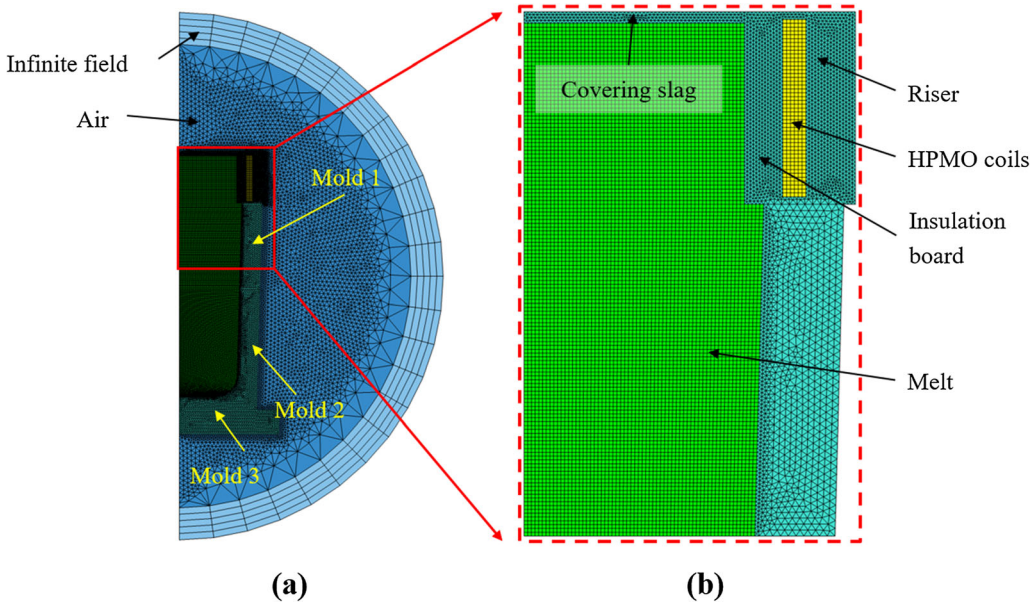

Fig. 3—Equal-proportion two-dimensional symmetrical model (with an HPMO coil): (*a*) grids comprising the model of the ingot treated by HPMO; (*b*) grids for the liquid steel, casting model, and HPMO coils.

When large free grains encoutere small grains, either small fragements or newly formed small grains, grain ripening occurs. Leading to the growth of larger grains and dissolution of smaller grains.[32,33] Still, a large number of small grains are likely to survive and grow into equiaxed grains eventually. It is believed that the application of HPMO increases the population of free grains in the ingot, leading to an expanded fine equiaxed zone in the ingot and improved mass feeding during the solidification of the ingot which are beneficial in reducing porosity and in avoiding crack formation during the solidification of the ingot. In the previous study,[34] PMO-induced electromagnetic fields and forced flow in liquid metal have been systematically investigated by performing numerical simulations and corresponding experimental measurements. The results of numerical simulations have been confirmed by magnetic and melt flow measurements.

IV. INDUSTRIAL EXPERIMENTS

A. *Experimental Process*

18-tonnes 18CrNiMo gear steel ingots were produced using a bottom-pouring process. The pouring temperature was 50 °C above the liquidus of the steel. One ingot was allowed to solidify naturally with its riser in a normal cast iron riser mold. Another ingot was treated by HPMO (for 8.5 h) 1 h after being poured. Figure 10(a) shows the experimental HPMO treatment system.

Figure 10(b) shows the locations of sampling in forging billets. First, the ingot was hot forged to generate billets of 580 mm diameter. Second, round slices were obtained from three positions: namely bottom slice, central slice, and top slice taken from 30 cm from the bottom; at the center; and 30 cm from the top of a billet, respectively. The top slice was originally in the riser on top of the ingot. Rectangular bars (width = 30 mm, thickness = 30 mm) were cut along the billet diameter. Next, chemistry specimens were drilled from the bars (using a drill bit of 5 mm diameter) at 15-mm intervals for measuring the carbon content by a CS2800 infrared carbon and sulfur analyzer (NCS Testing Technology Co., Ltd., China). Then, bars were cut into five samples (length = 60 mm; width = 30 mm; height = 20 mm) from the edge to the center. These samples were ground, polished, and etched by a 1:1 picric acid/alcohol solution for 40 s. A metallographic microscope (Imager.A2m, Carl Zeiss AG, Germany) was used to observe the microstructure. Samples (10 mm×10 mm) were cut from two points: at 1/2 the radius of the forging billet, and at the center of the forging billet, respectively, for inclusion measurement. Inclusions were counted on the polished specimens. The visual fields with most inclusions were captured with 100× magnification. Five sets of 0.5 mm^2 metallographic photos were taken from each sample to count the number of inclusions larger than 1 μm. In addition, Dog-bone shaped tensile test bars, shown in Figure 10(c), were machined along the radial direction of round slices.

V. RESULTS AND DISCUSSION

A. *Microstructure*

Light microscopy images taken at the edge and in the center of the bottom slices of two forged billets revealed that the solidified microstructure of the billet treated with HPMO was much finer, more compact, and more uniform (especially at the center) than that of the billet without subjected to HPMO (Figures 11 and 12).

Table IV. Heat Transfer Boundary Conditions

Position	Heat Transfer Coefficient/ $W \cdot m^{-2} \cdot K^{-1}$
Melt/Mold 1	As Shown in Fig. 4
Melt/Mold 2	As Shown in Fig. 4
Melt/Mold 3	800
Melt/Riser	30
Melt/ Covering Agent	5
Riser/Air	20
Mold/Air	100
Covering Agent/Air	20
Mold/Ground	200

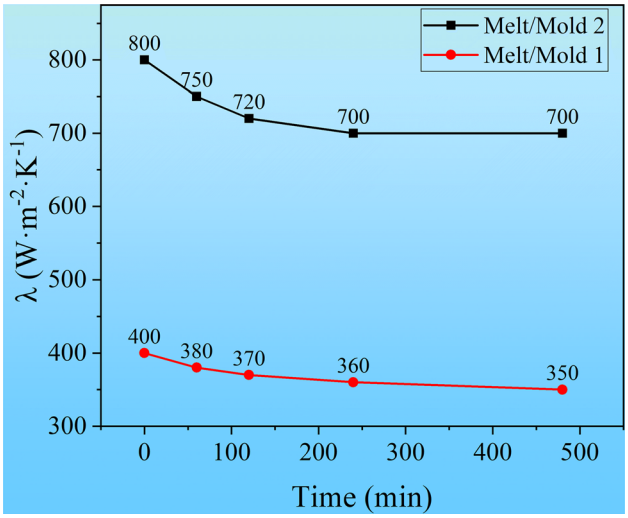

Fig. 4—Heat transfer coefficients of Molds 1 and 2 over time.

Images taken at the edges of the middle slice (1/2 height) of forged billets showed that the parallelism of columnar dendrites was much greater in the non-HPMO-treated billet (Figure 13) than that in the HPMO-treated billet. In the HPMO-treated billet, dendritic grains were more random in their growth directions, the secondary arms of the dendritic grains were coarser, and the mixed grain zone was larger than that in the non-HPMO-treated billet. The increased size of the mixed grain zone may have been the result of 1) a significant increase in the number of nuclei and 2) the enhanced circulation of a large number of free grains. According to simulation results on flow field and temperature field shown in Figures 8 and 9, the combination of circulation and Joule heat effect leads to temperatures higher near the outside of the metal in the riser than that in the center of the riser, thus increasing local solidification times and causing dendritic grains to become coarser. Images taken in the center of the middle slice (1/2 height) shown in Figure 14 demonstrate that the microstructure of the HPMO-treated specimen was fine, dense, and flawless, while the microstructure of the non-HPMO-treated specimen was clearly coarser and contained large micro-shrinkage cavities and central cracks.

Figures 15 and 16 illustrate light microscopy images taken at the edges and in the center of the riser (top level) demonstrating that HPMO improves the microstructure of forged billets. The microstructure of the non-HPMO-treated billet exhibited non-directional fine dendritic grains and included two cracks (Figure 15(a)). In contrast, the microstructure of the HPMO-treated billet was compact, with no visible cracking (Figure 15(b)). The direction of growth of dendritic grains near the edge of billet clearly changed as

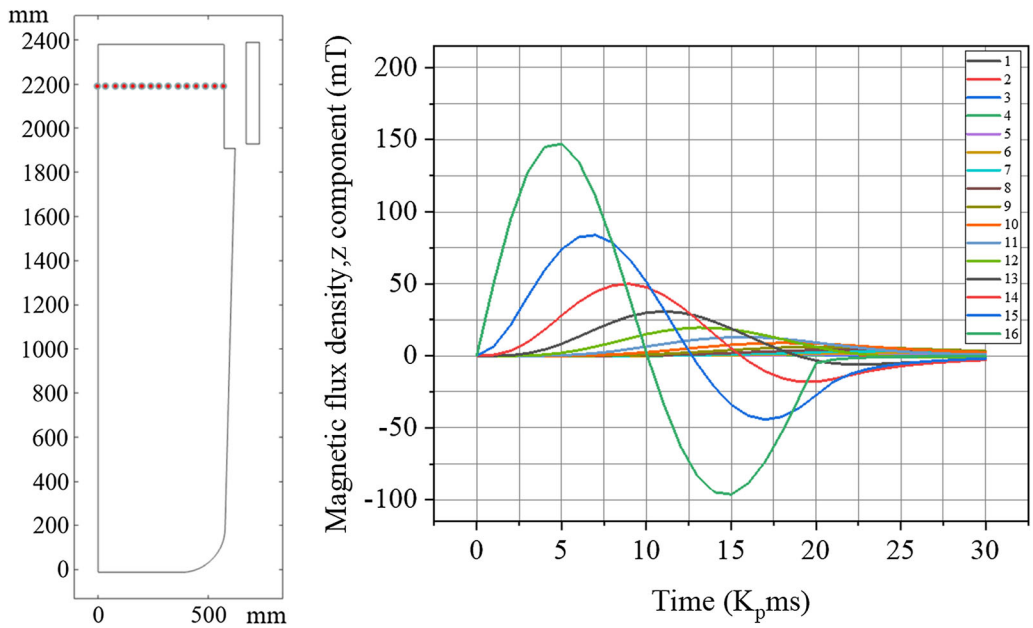

Fig. 5—Distribution of the magnetic flux density along the radial direction at the center of the coil's height during HPMO. The numbers in right-hand figure indicate the location in an ingot shown in the left-hand figure.

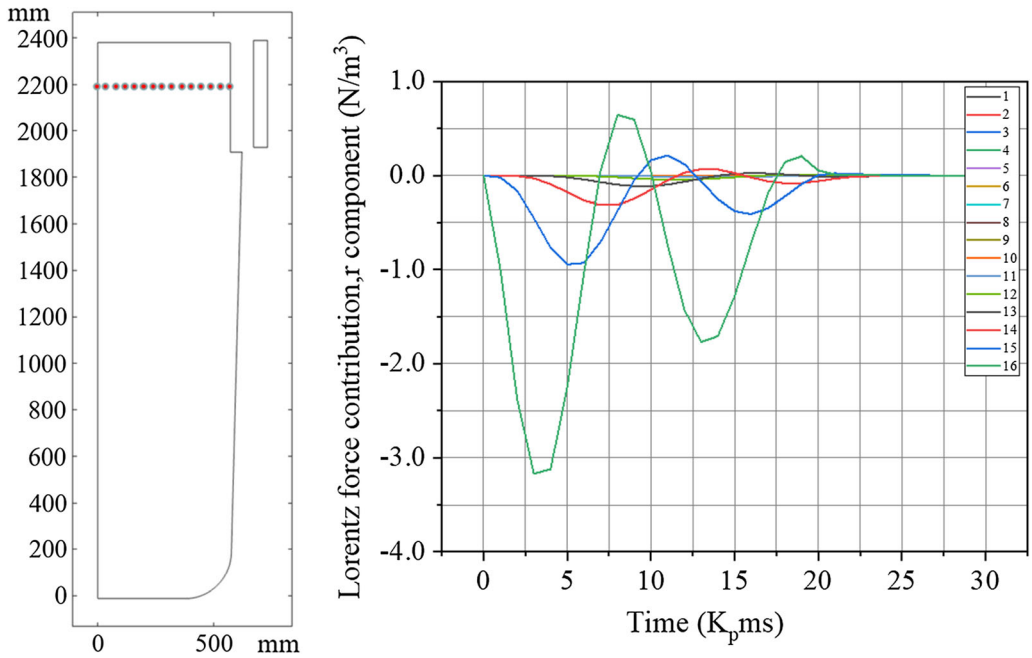

Fig. 6—Variations in the electromagnetic force from the center of the melt to the edge during one pulse period of HPMO.

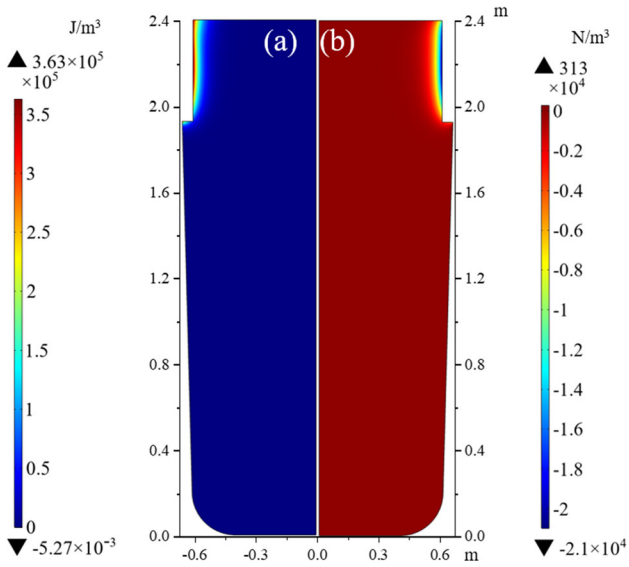

Fig. 7—Distributions of the mean Joule heat (far left scale) and electromagnetic force (far right scale) in the ingot during one pulse. The dimension of the ingot is in meters (m). The length is about 2.4 m and the maximum diameter is about 1.2 m.

well. Considering that columnar grains grow under convection, the change that we observed in the growth directions of dendritic grain must have reflected a change in the flow direction of liquid steel. Such an assumption is supported by our simulation results (Figure 8). Magnetic field strength and flow are sharply attenuated by the severe shielding of the pulsed magnetic field that resulted from the formation of a solidified shell. Dendrite growth direction was mostly orderly in the range of 31 mm from the HPMO energy source and mostly disorderly at about 54 mm. In the center of the riser in the HPMO-treated billet, coarse dendritic grains did not form at all, and the microstructure was fine and compact (Figure 16).

To evaluate the degree of refinement of microstructure, we measured the mean grain size of HPMO-treated and non-HPMO-treated billets at the center of each of three slices (bottom, 1/2 height, riser). The mean grain sizes in the HPMO-treated billet were 0.4 in the bottom slice, 1.0 at 1/2 height, and 0.8 in the riser, compared to 2.3 mm, 2.3 mm, and 2.2 mm, respectively, in the corresponding slices of non-HPMO-treated billet (Figure 17). In other words, the use of HPMO resulted in reductions in grain size about 83 pct, 56 pct, and 64 pct in those corresponding locations, indicating that grain densities increased more than tenfold with HPMO-treatment. Although the analysis of grain size statistics may have been complicated by the various branching shapes of dendritic grains, the overall grain refinement effect of HPMO is undeniable. Much finer equiaxed grains were obtained in samples taken from all points in the billets, especially those in the bottom slice.

Simulated maximum flow velocities in the HPMO-treated ingot, calculated at the wall of the riser, were about 110 mm/s 1 h after pouring and 70 mm/s 2 h after pouring (Figure 8). The corresponding maximum flow velocities under natural convection would be only about 8 mm/s and 7 mm/s. The strengthened convection caused by HPMO must have accelerated the heat dissipation of the liquid steel, thus causing the superheat to disappear quickly, promoting grain nucleation and preventing the remelting of nuclei. Nucleation is first induced near the walls because, during solidification, the temperature near the wall is lower than in the center. We deduced that the oscillation effect of HPMO causes nucleated grains to fall off the walls into the melt, where

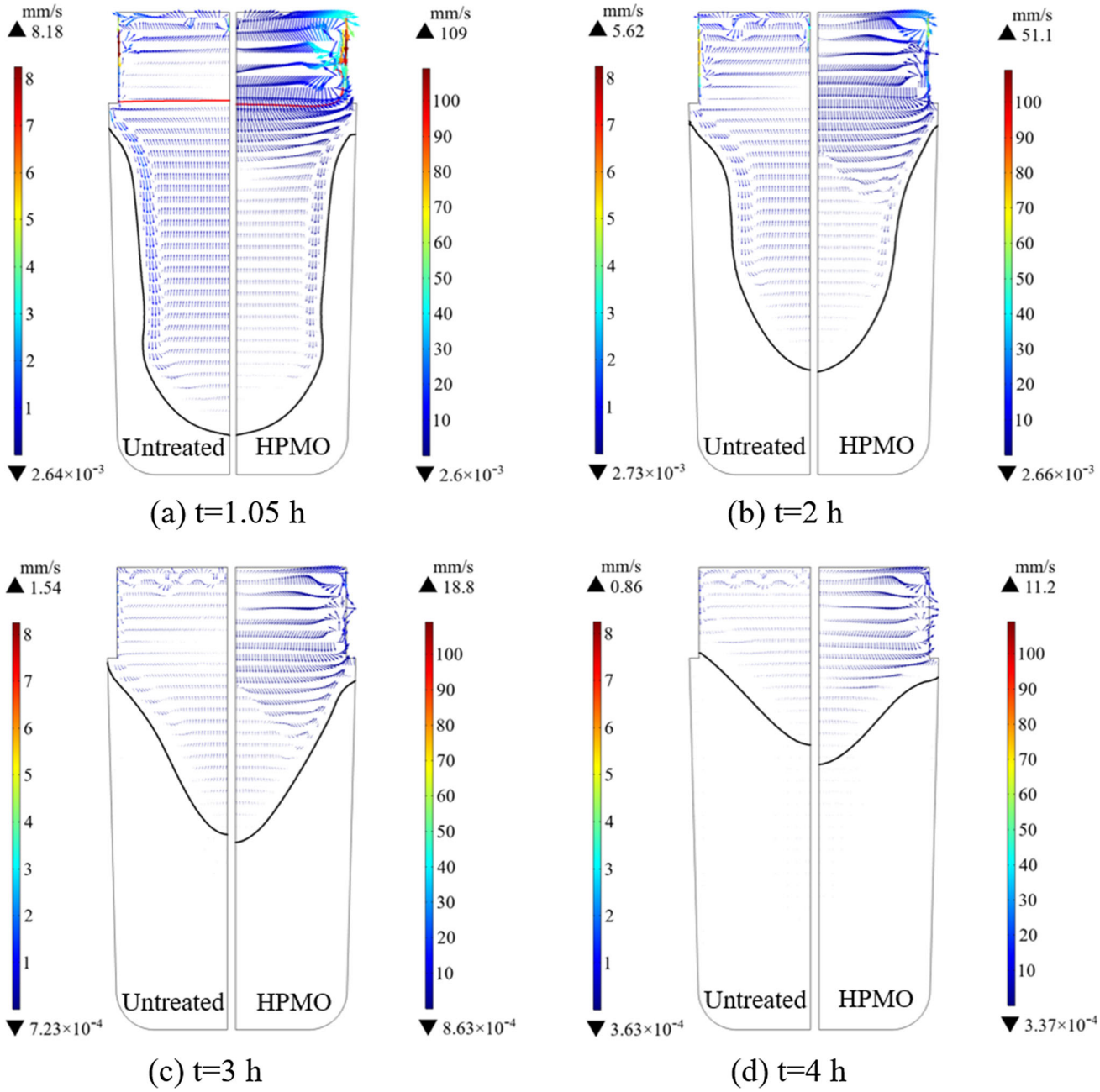

Fig. 8—Distribution of the flow fields in the ingot with and without HPMO at various times. (*a*) t = 1.05 h, (*b*) t = 2 h, (c) t = 3 h, and (d) t = 4.0 h.

the combination of natural convection and the HPMO-caused flow carries them toward the ingot center, where they sink to the freezing fronts. This process would significantly enhance equiaxed grain refinement near the bottom of the ingot[35]. During the early stage of solidification (within 1 h as shown in Figure 8(a)), the temperature at the center remained slightly higher than that at the edges where the melt was still superheating. As a result, free dendrites could not easily grow in the liquid core, and they might even undergo remelting and fragmentation. Consequently, the grains deposited at the bottom of the ingot were the smallest (Figure 17). As the solidification process continued and the temperature decreased, the velocities and regions influenced by the riser decreased significantly. The maximum velocity of liquid steel in the HPMO-treated ingot, however, was still significantly higher than that in the non-HPMO-treated ingot (see Figure 8). Accordingly, the promotion of grain movement was obvious with HPMO. At the stage 2–3 h after pouring, the superheat of the liquid steel in the riser has been exhausted, and the free grains gradually grew during the circulation and settling processes. Therefore, the grain size was larger than that at the initial stage of solidification. This is also the reason that the equiaxed grain size at 1/2 the height of the billet was larger than that at the bottom.

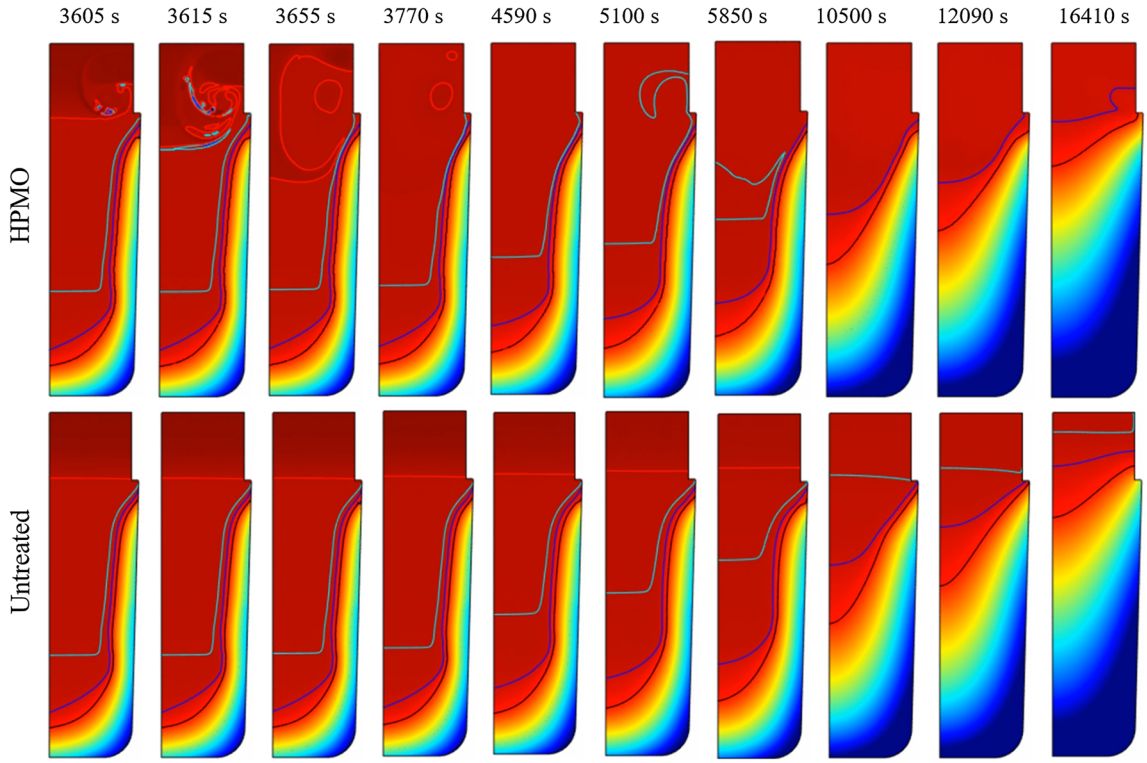

Fig. 9—Temperature fields and solid fractions (provide temperature bars, etc) in ingots with and without HPMO at different solidification times.

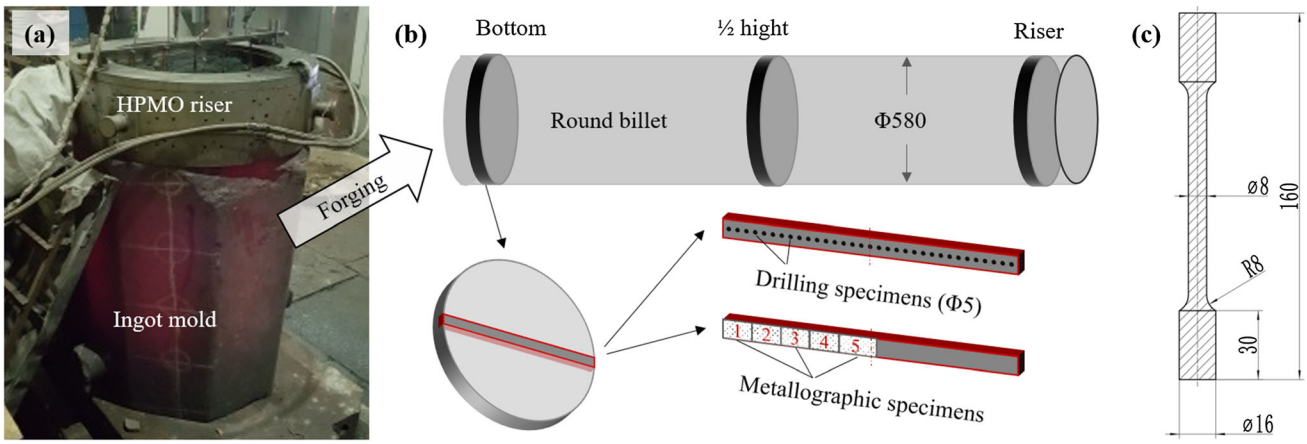

Fig. 10—(*a*) Experimental HPMO treatment process, (*b*) locations of sampling from a forged billet, and (*c*) dimensions of a tensile specimen.

B. *Carbon Macrosegregation*

We considered that the carbon segregation index K is the most convenient parameter to describe carbon macro-segregation:

$$K = \left(C_i/\overline{C}\right) \qquad [1]$$

where C_i is the carbon content at position i across the diameter of a slice sample, and $\overline{C}$ is the weighted average of carbon contents over all tested points. The $\overline{C}$ value was calculated by:

$$\overline{C} = \frac{\sum C_i(r_i + 2.5)^2}{\sum (r_i + 2.5)^2} \qquad [2]$$

where r_i is the distance in mm between the center of the sampling position and the center of the ingot. The drill radius was 2.5 mm, as shown in Eq. [2].

The values for K measured along the radial direction in round billets with or without HPMO showed very different trends in different height locations (Figure 18). Except in the edge zones, negative segregation existed at

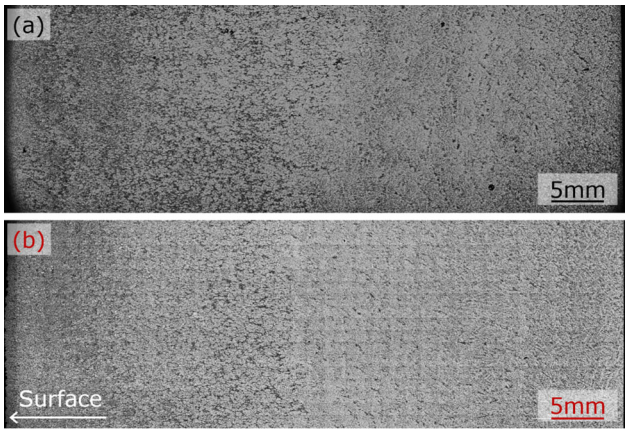

Fig. 11—Microstructures of samples taken at the edge of the bottom slice of forged billets (*a*) without HPMO; (*b*) with HPMO.

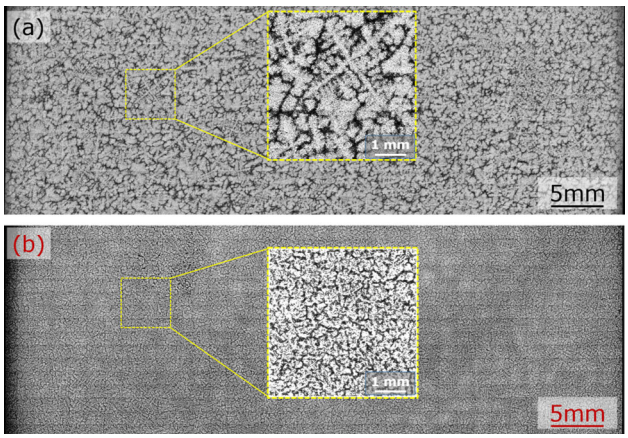

Fig. 12—Microstructures of samples taken at the center of the bottom slice of forged billets (*a*) without HPMO; (*b*) with HPMO.

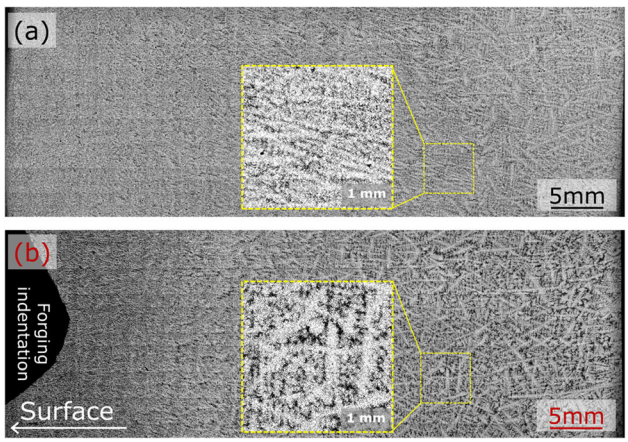

Fig. 13—Microstructures in samples taken at the edge of the central slices of forged billets (*a*) with and (*b*) without HPMO.

the bottom of both billets, where K undulated slightly. At the bottom of the billet without HPMO, carbon segregation followed an inverted W shape, in that the carbon content at 1/2 the radius was significantly higher than at the center. At the bottom of the billet with

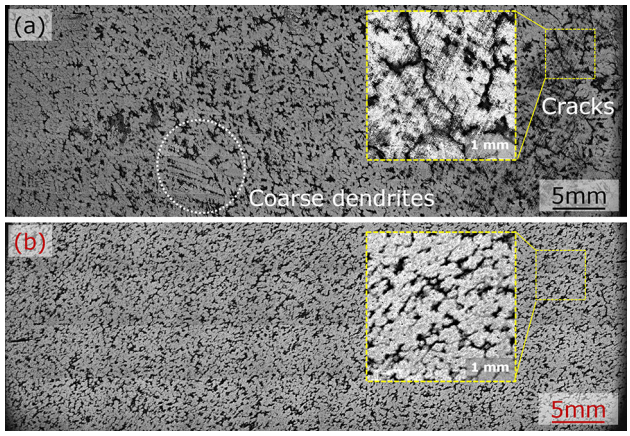

Fig. 14—Microstructures of samples taken in the central slices of the forged billets (*a*) with and (*b*) without HPMO.

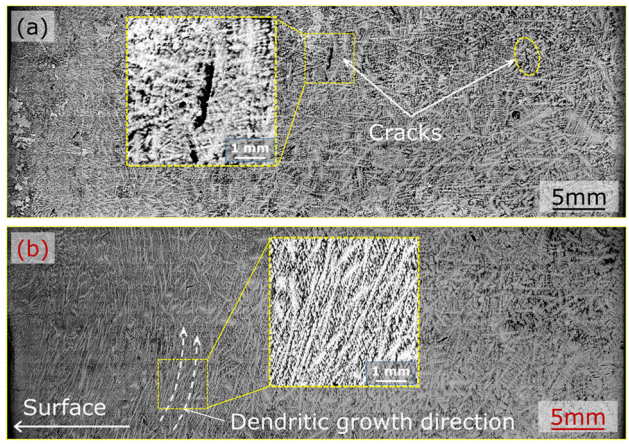

Fig. 15—Microstructures of samples taken from the edge of the top slices (which was in the riser) of forged billets (*a*) with HPMO and (*b*) without HPMO.

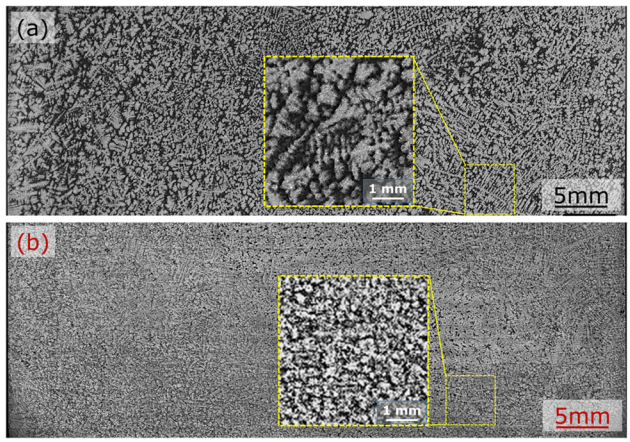

Fig. 16—Microstructures of samples taken from the center of the top slices (which were in the riser) of forged billets (*a*) with HPMO and (*b*) without HPMO.

HPMO, carbon distribution was more uniform. There were no significant differences in carbon content along the radial direction, with the exception of some positive

segregation observed at the edges. Microstructural observations shown in Figure 12 indicated that the equiaxed grains at the bottom of this billet were significantly refined. Compared to the billet without HPMO, carbon negative segregation was slightly higher in the billet with HPMO and the variation in segregation between the center point and 1/2 the radius was significantly lower.

By contrast with the bottom of each billet, where little channel segregation was observed, samples taken at the center slice (1/2 height) showed the most severe carbon segregation of the billets investigated in this study. Segregation in this location was associated with channel segregation occurring at 1/2 the radius. In the billet with HPMO, carbon distribution was significantly homogenized, leading to a 50 pct decrease in the maximum carbon segregation value (from 32 to 16 pct). Previous researchers have identified inclusion flotation as an important cause of channel segregation.[4] This implies that a lower density of inclusions, which we observed in our HPMO-treated ingot, would reduce channel segregation (Figure 19). We speculated that grain refinement of dendrites in the mushy zone would further contribute to a reduction in channel segregation.

In the center of samples taken from the risers (the top slice) of each billet, severe positive segregation occurred, more with HPMO than without. It is apparent that HPMO brought about enhanced nucleation in the riser. Meanwhile, the partitioning during solidification that was also enhanced led to solute enrichment in the liquid steel as free grains leave the riser region. The resulting increase in the solute content of carbon reduced the density of the liquid steel, thus inducing an upward flow. Double circulation generated by HPMO at the riser benefited the retention of C-rich, low-density liquid steel in the upper circulation region, thus reducing mass transfer from the riser region to the bottom region of the ingot. The carbon content in the riser layer thus increases gradually, ultimately forming a region of severe positive segregation. Because of severe carbon concentration, the risers must be excised during utilization.

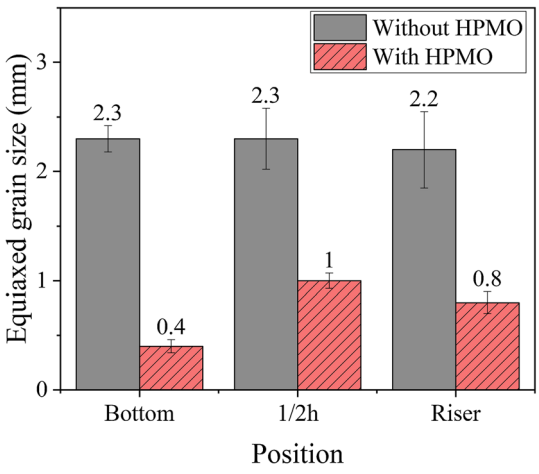

Fig. 17—Mean grain sizes in the center of slice taken from various location in the forged billets with and without HPMO treatment.

C. *Inclusions*

At the 1/2 radius of the cylindrical billets, the number of inclusions was generally consistent in HPMO and non-HPMO billets; both contained more inclusions at the riser than at that at 1/2 height (Figure 19(a)).

In the center of the billets, the number of inclusions in the billet without HPMO increased from the bottom to the riser, while in the billet with HPMO the opposite was true—the number of inclusions decreased from the bottom to the riser (Figure 19(b)). The mean number of inclusions estimated at different locations in the center of the HPMO-treated billet was reduced by 47 pct from 46 to 24 mm^{-2}. The reduction was even more obvious in the riser. The reduced number of inclusions in the center of the billet can be attributed to the fact that HPMO-induced forced convection must have caused the inclusions to float upward. Also, because of grain refinement brought about by HPMO, the settling grains, being smaller, must have become less likely to capture

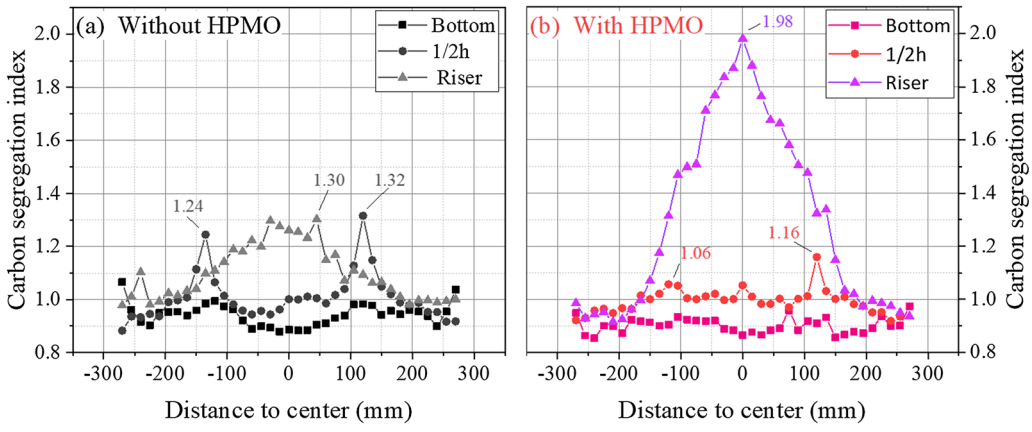

Fig. 18—Carbon segregation along the radial direction at the bottom, 1/2 height, and riser slices of the forged billet (*a*) without and (*b*) with HPMO.

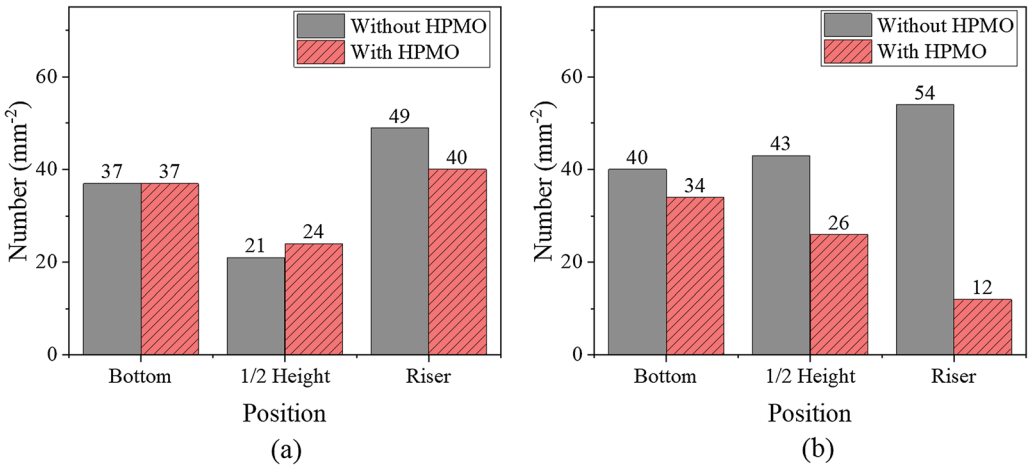

Fig. 19—The number of inclusions per unit area at different location of the billets: (*a*) 1/2 radius; (*b*) center.

whatever inclusions passed nearby, so these inclusions continued to float to the top where they could be easily skimmed off.

D. *Mechanical Properties*

To select samples for tensile tests of both HPMO and non-HPMO billets, we first cut one slice from the bottom of each billet and another from the 1/2 height. From each slice, we cut samples from three locations with different radial carbon segregation indices (Figure 20). As in Table V, we found that tensile test results were more uniform in the HPMO treated billet, whose ultimate tensile strength showed a change less than 4.8 pct and whose elongation values were all greater than 15 pct, with variations less than 8.9 pct. The values for reduction-in-area at fracture were greater than 55 pct, with variations less than 5.2 pct.

The untreated billet, on the other hand, showed large variations in values for ultimate tensile strength, elongation, and reduction-in-area at fracture. A sample taken from location V in Figure 20 of the center slice of the untreated billet showed exceptionally low elongation (4 pct) with characteristics of brittle fracture. Result of re sampling at adjacent locations (V') still showed a low elongation (6 pct) with brittle fracture characteristics. We attributed this embrittlement to the phenomenon of central crack and porosity that we had previously observed in macroscopy images of the untreated billet (Figure 14).

In any case, the higher the carbon content (*i.e.*, the more pronounced the positive segregation), the greater the ultimate tensile strength of the test bar; the lower the carbon content (*i.e.*, the more pronounced the negative segregation), the lower the ultimate tensile strength of the test bar. We concluded that HPMO treatment produced greater uniformity in both plasticity and strength distribution.

VI. CONCLUSIONS

Our method, Hot-Top Pulsed Magneto-Oscillation (HPMO), has been shown to effectively improve the microstructure and macrosegregation of heavy ingots. Our main conclusions, based on results of industrial experiments on 18-tonne ingots, are as follows:

(1) The coupling effects induced by HPMO during ingot solidification (increased nucleation, forced convection, and induction heating) significantly affected the ingots by refining solidification structure, reducing macrosegregation, and strengthening the feeding effect of the riser, thus improving overall material yield.
(2) The results of numerical simulations indicated that the flow field in the melt reached stabilization after 50 s of HPMO treatment. This flow field induced three large circulation patterns in the upper, middle, and lower regions. The maximum flow velocity at the riser edge reached 110 mm/s, which was much higher than the natural convection observed in untreated melt.
(3) Free grains in the HPMO-treated ingot were about 10 times more likely than that in the untreated one. These free grains tend to be deposited as sediment at the bottom freezing front, becoming small equiaxed grains in the center region of the ingot. The results of industrial tests demonstrated that HPMO significantly refined the microstructure of the ingot, leading to a 56–83 pct reduction of equiaxed grain size in the center of the ingot.
(4) Cracks were observed in the center at the 1/2 height of the untreated ingot, but there were no central crack defects in the HPMO-treated ingot. Cracking was apparently reduced by a mass feeding effect at the riser and by the formation of small equiaxed grains in the mushy zone.
(5) Carbon distribution in the HPMO-treated ingot became more uniform at the bottom and at the 1/2 height of the billet, leading to more uniform mechanical properties than the untreated ingot. The maximum segregation index at the 1/2 height de-

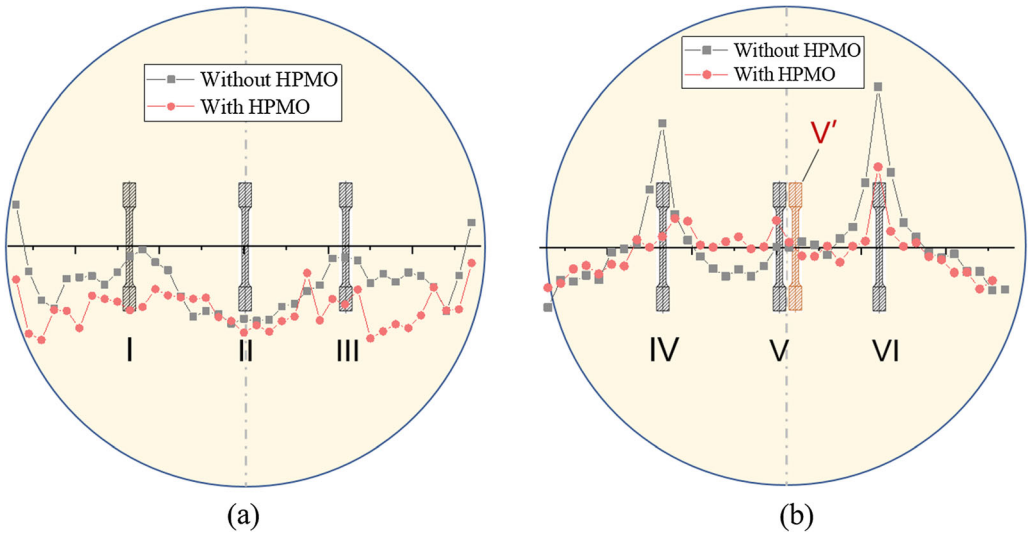

Fig. 20—Schematic diagrams of the sampling position and its relationship with the radial distribution of carbon segregation index. (*a*), bottom slice and (*b*) central slice, *i.e.*, 1/2 height. of dog-bone shaped tensile test bar. V and V' in (*b*) are locations in the un-treated ingot where low elongation values were measured.

Table V. Mechanical Properties of the Test Bar Sampled from Position on th Bottom and the Central Slice of Forged Billets

	Ultimate Tensile Strength (Mpa)		Yield Strength (Mpa)		Elongation (pct)		Reduction of Area (pct)	
Position	Without HPMO	With HPMO	Without HPMO	With HPMO	Without HPMO	With HPMO	Without HPMO	With HPMO
I	685	671	476	441	16	18	56	58
II	656	668	445	419	18	18	58	58
III	684	672	474	448	17	18	59	57
IV	737	691	501	486	16	17	60	57
V	682	687	479	491	4	16	3	60
V'	686		483		6		4	
VI	760	703	519	543	16	16	58	58

creased by a 50 pct (from 32 pct in the untreated billet to 16 pct in the treated billet).

(6) Carbon was enriched in the riser of the HPMO-treated ingot. The riser was likely out of the chemical specification of the steel and has to be sectioned off in applications.

ACKNOWLEDGMENTS

This work was financially supported by the NSFC [Grant Number 52130109]. A portion of the work was undertaken in the National High Magnetic Field Laboratory, which is supported by NSF DMR-1157490 and the State of Florida. The authors gratefully acknowledge the professional and careful experimental work of Wenjun Lv (Daye Special Steel Co. LTD), Huicheng Li and Hui Shao (Center for Advanced Solidification Technology, Shanghai University). We also thank Drs. Suzanne Adam and Mary Tyler for editing.

CONFLICT OF INTEREST

The authors declare that they have no known competing financial interests or personal relationships that could have appeared to influence the work reported in this paper.

SUPPLEMENTARY INFORMATION

The online version contains supplementary material available at https://doi.org/10.1007/s11663-024-03019-z.

REFERENCES

1. G. Lesoult: Macrosegregation in steel strands and ingots: Characterisation, formation and consequences. *Mater. Sci. Eng. A*, 2005, vol. 413–14, pp. 19–29.
2. M.C. Flemings: Our understanding of macrosegregation: past and present. *ISIJ Int.*, 2000, vol. 40(9), pp. 833–41.
3. M.C. Flemings: *Solidification processing*, McGraw- Hill, New York, 1974.

4. D. Li, X. Chen, P. Fu, X. Ma, H. Liu, Y. Chen, et al.: Inclusion flotation-driven channel segregation in solidifying steels. *Nat. Commun.*, 2014, vol. 5, p. 5572.
5. D.G. Eskin, Q. Du, and L. Katgerman: Relationship between shrinkage-induced macrosegregation and the sump profile upon direct-chill casting. *Scr. Mater.*, 2006, vol. 55(8), pp. 715–18.
6. D. Sun, J. Zhang, X. Yang, and K. Mu: Exothermic and insulating riser design of gear ring seat casting based on any casting. *J. Phys. Conf. Ser.*, 2018, vol. 1064(1), p. 12005.
7. O. Yücel, A. Turan, and K.C. Candeğer: Effects of changing size-weight parameters on the temperature dependent exothermic riser sleeve properties. *Eurasian Chem. Technol. J.*, 2018, vol. 20(1), pp. 17–21.
8. O. Yucel, A. Turan, and K.C. Candeger: Optimization of exothermic riser sleeve design parameters. *Miner. Metals Mater. Ser.*, 2018, https://doi.org/10.1007/978-3-319-72138-5_35.
9. W.T. Tu, H.F. Shen, and B.C. Liu: Modelling of macrosegregation in a 231-ton steel ingot with multi-pouring process. *Mater. Res. Innovations*, 2015, vol. 19(4), pp. S59-63.
10. O. Kudryashova, M. Khmeleva, P. Danilov, V. Dammer, A. Vorozhtsov, and D. Eskin: Optimizing the conditions of metal solidification with vibration. *Metals.*, 2019, vol. 9(3), p. 366.
11. V. Promakhov, M. Khmeleva, I. Zhukov, V. Platov, A. Khrustalyov, and A. Vorozhtsov: Influence of vibration treatment and modification of A356 aluminum alloy on its structure and mechanical properties. *Metals.*, 2019, vol. 9(1), p. 87.
12. B. Sang, X. Kang, and D. Li: A novel technique for reducing macrosegregation in heavy steel ingots. *J. Mater. Process. Technol.*, 2010, vol. 210(4), pp. 703–11.
13. D.M. Gao, Z.J. Li, Q.Y. Han, and Q.J. Zhai: Effect of ultrasonic power on microstructure and mechanical properties of AZ91 alloy. *Mater. Sci. Eng. A*, 2009, vol. 502(1–2), pp. 2–5.
14. X. Jian, H. Xu, T.T. Meek, and Q. Han: Effect of power ultrasound on solidification of aluminum A356 alloy. *Matt. Leeter.*, 2005, vol. 59(2–3), pp. 190–93.
15. Q.Y. Han: Ultrasonic processing of materials. *Metall. Mater. Trans. B*, 2015, vol. 46, pp. 1603–14.
16. D. Eskin and F. Wang: Joint effect of ultrasonic vibrations and solid metal addition on the grain refinement of an aluminium alloy. *Metals.*, 2019, vol. 9(2), p. 161.
17. Y. Wan, M. Li, L. Chen, Y. Wu, J. Li, H. Pan, and W. Zhong: Effect of final electromagnetic stirring parameters on central cross-sectional carbon concentration distribution of high-carbon square billet. *Metals.*, 2019, vol. 9(6), p. 665.
18. Q. Fang, H. Ni, B. Wang, H. Zhang, and F. Ye: Effects of EMS induced flow on solidification and solute transport in bloom mold. *Metals.*, 2017, vol. 7(3), p. 72.
19. P. Mikolajczak: Microstructural evolution in AlMgSi alloys during solidification under electromagnetic stirring. *Metals.*, 2017, vol. 7(3), p. 89.
20. N. Li, L. Zhang, R. Zhang, P. Yin, H. Xing, and H. Wu: Research on grain refinement in hypoeutectic Al-Si Alloy during solidification under an alternating electric current pulse. *Metals.*, 2019, vol. 9(5), p. 571.
21. Y. Zhang, C. Ye, Y. Xu, H. Zhong, X. Chen, X. Miao, et al.: Influence of growth velocity on the separation of primary silicon in solidified Al-Si hypereutectic alloy driven by a pulsed electric current. *Metals.*, 2017, vol. 7(6), p. 184.
22. Y. Zhang, X. Cheng, H. Zhong, Z. Xu, L. Li, Y. Gong, et al.: Comparative study on the grain refinement of Al-Si alloy solidified under the impact of pulsed electric current and travelling magnetic field. *Metals.*, 2016, vol. 6(7), p. 170.
23. F. Ren, J. Li, H. Ge, D. Cai, Q. Hu, and J. Li: A comprehensive study of layer casting process by a four-phase filling-solidification model. *J Mater Process Tech.*, 2020, vol. 284, p. 116737.
24. L. Jun, W. Junge, R. Fengli, G. Honghao, H. Qiaodan, X. Mingxu, et al.: Experimental and numerical simulation study on layer casting method for composition homogeneity on ingot casting. *Acta Metall. Sin.*, 2018, vol. 54, p. 118.
25. Y. Gong, J. Luo, J. Jing, Z. Xia, and Q. Zhai: Structure refinement of pure aluminum by pulse magneto-oscillation. *Mater. Sci. Eng. A*, 2008, vol. 497(1–2), pp. 147–52.
26. J. Zhao, J. Yu, K. Han, H. Zhong, R. Li, and Q. Zhai: Effect of coil configuration design on Al solidified structure refinement. *Metals.*, 2020, vol. 10(1), p. 153.
27. H. Li, Z. Liu, R. Li, Y. Gong, Z. Xu, and Q. Zhai: Distribution of nonmetallic inclusions in molten steel under hot-top pulsed magneto-oscillation treatment. *J. Iron. Steel Res. Int.*, 2018, vol. 25(8), pp. 867–76.
28. X. Liao, Q. Zhai, J. Luo, W. Chen, and Y. Gong: Refining mechanism of the electric current pulse on the solidification structure of pure aluminum. *Acta Mater.*, 2008, vol. 55(9), pp. 3103–09.
29. W.D. Bennon and F.P. Incropera: A continuum model for momentum, heat and species transport in binary solid-liquid phase change systems—I: model formulation. *Int. J. Heat Mass Transfer.*, 1987, vol. 30(10), pp. 2161–70.
30. J. Ni and F.P. Incropera: Extension of the continuum model for transport phenomena occurring during metal alloy solidification—II: microscopic considerations. *Int. J. Heat Mass Transfer.*, 1995, vol. 38(7), pp. 1285–96.
31. I. Edry, T. Mordechai, N. Frage, and S. Hayun: Effects of treatment duration and cooling rate on pure aluminum solidification upon pulse magneto-oscillation treatment. *Metall. Mater. Trans. A*, 2016, vol. 47(3), pp. 1261–67.
32. Q. Han: Dendritic features of the solidification structure in a large AA3004 direct chill (DC) cast ingot. *Metall. Mater. Trans. B*, 2022, vol. 53(2), pp. 786–97.
33. Q.Y. Han: The role of solutes in grain refinement of hypoeutectic magnesium and aluminum alloys. *JMA.*, 2022, vol. 10(7), pp. 1846–56.
34. Y.Y. Xu, J. Zhao, C.Y. Ye, et al.: Distributions of electromagnetic fields and forced flow and their relevance to the grain refinement in Al–Si alloy under the application of pulsed magneto-oscillation. *Acta Metall. Sin.*, 2022, vol. 35, pp. 254–74.
35. F. Zhang, H.G. Zhong, Y.Q. Yang, et al.: Improving ingot homogeneity by modified hot-top pulsed magneto-oscillation. *J. Iron. Steel Res. Int.*, 2022, vol. 29(12), pp. 1939–50.